ISSN 1070-3632, Russian Journal of General Chemistry, 2019, Vol. 89, No. 2, pp. 330–338. © Pleiades Publishing, Ltd., 2019.

Structural Characterization and Second-Order Nonlinear Optical Behavior of Metal Complexes of Ferrocene Derivative

P. Deveci[a]*, B. Taner[a], E. Özcan[a], Z. Kılıç[b], M. Karakaya[c], and A. Karakas[d]

[a] *Selcuk University, Faculty of Science, Department of Chemistry, Konya, 42031 Turkey*
**e-mail: pervindeveci@gmail.com*

[b] *Ankara University, Faculty of Science, Department of Chemistry, Tandogan, Ankara, 06100 Turkey*

[c] *Sinop University, Faculty of Engineering and Architecture, Department of Energy Systems, Sinop, Turkey*

[d] *Selcuk University, Faculty of Science, Department of Physics, Konya, 42031 Turkey*

Received November 28, 2018; revised February 8, 2019; accepted February 8, 2019

Abstract—In this manuscript, a ferrocene-linked *vic*-dioxime ligand (LH_2) and its metal complexes [$Ni(LH)_2$, $Cu(LH)_2$, $Co(LH)_2(H_2O)_2$, $Cd(LH)(H_2O)(Cl)$, and $Zn(LH)(H_2O)(Cl)$] are synthesized, and their structures are studied by spectral methods. Redox behavior of the compounds is studied by cyclic voltammetry (CV). For approaching microscopic second-order nonlinear optical (NLO) behavior of the synthesized ligand and its diamagnetic Cd(II), Zn(II), Ni(II) complexes, the electric dipole moment μ, static dipole polarizability α, and first hyperpolarizability β values are computed using ab-initio quantum chemical procedure [finite field (FF)]. The accumulated data indicate that the compounds exhibit non-zero quadratic hyperpolarizability tensor components, implying microscopic NLO phenomena. The HOMOs, LUMOs and the HOMO–LUMO band gaps for first and second frontier orbitals of LH_2 ligand and its Cd(II), Zn(II), Ni(II) complexes are evaluated by means of the Hartree-Fock (HF) method.

Keywords: metal complex, redox property, ferrocene, nonlinear optics, finite field, HOMO–LUMO

DOI: 10.1134/S1070363219020269

INTRODUCTION

Functionalization of organometallic derivatives of ligands containing redox active ferrocene on their periphery is currently an active area of research owing to the potential applications of such systems in optics and electronics [1–3], as biosensors [4–6], semiconductors [7–9], catalysis [10, 11], bioorganometallic materials [12, 13], and in nonlinear optics [14, 15]. *vic*-Dioximes [16, 17] can form different types of complexes with metal ions [18,19]. Cobaloximes are used as model compounds in the studies of vitamin B_{12} coenzyme [20]. Ni(II) Complexes of *vic*-dioxime ligands also attracted considerable attention [21]. NLO materials play an important role as active components in a large range of applications such as optical communications, optical storage, optical computing, harmonic light generation, frequency mixing, and optical switching [22]. Incorporation of a heavy atom in transition metal complexes introduces more sublevels into the energy hierarchy as compared to organic molecules with the same number of skeletal atoms, and this permits a greater number of allowed electronic transitions and, hence, enhances the NLO response. Utilization of ab initio methods in calculation of NLO characteristics of transition metal complexes has been exploited to a low extent because of heavy computational cost in handling these systems. However, we have made an attemp to utilize *ab initio* methods for studying NLO characteristics. One of the purposes of this work was also obtaining the second-order NLO behavior of LH_2 ligand and its diamagnetic Cd(II), Zn(II), Ni(II) complexes. We report here the electric dipole moments, static dipole polarizabilities and first hyperpolarizabilities computed by the FF procedure. In addition to NLO properties, the HOMO–LUMO energies and gaps of the outermost molecular orbitals for LH_2 ligand and its Cd(II), Zn(II) and Ni(II) complexes were calculated by the HF method.

EXPERIMENTAL

β-Ferrocenylethylamine [23–25] and 4-(phenoxy)-chlorophenylglyoxime [26, 27] were synthesized as

reported. All other chemicals were purchased from Merck or Sigma-Aldrich.

Physical measurements. The CHN analysis was carried out on a LECO-932 model analyzer. FT-IR spectra were recorded on a Perkin-Elmer Spectrum 100 FT-IR spectrophotometer. NMR spectra were measured on a Varian Unity INOVA 500 spectrometer using DMSO-d_6 as a solvent. UV-Vis spectra were recorded on a Shimadzu UV-1700 spectrophotometer. MS spectra were measured on a Bruker Micro TOF LC-MS spectrometer. All electrochemical experiments were performed using a Gamry Reference 600 workstations (Gamry, Pennsylvania, USA) electrochemical analyzer (Model 600C series) equipped with BAS C3 cell stand. The working electrode was a bare glassy carbon disk (BAS Model MF-2012) with a geometric area of 0.027 cm^2. The reference electrode was Ag/Ag^+ (0.01 M) in nonaqueous media, and the counter electrode used was Pt wire.

Synthesis of the ligand LH_2. A solution of β-ferrocenylethylamine (1.15 g, 5 mmol) in 20 mL THF was added to a stirred mixture of 4-(phenoxy)chlorophenylglyoxime (1.45 g, 5 mmol) with TEA (0.7 mL, 5 mmol) in methanol (20 mL). The mixture was stirred at room temperature for 2 h and monitored by TLC using ethyl acetate–*n*-hexane (3 : 1) as an eluent. Upon completion of the process the solvent was evaporated. Purification of the residue by column chromatography on silica gel using ethyl acetate–*n*-hexane (3 : 1) as an eluent gave the *vic*-dioxime derivative LH_2. Yield 30%, mp 147°C. FT-IR spectrum, ν, cm^{-1}: 3344, 3229, 3067, 3037, 2917, 2855, 1651, 1609, 1588, 1507, 1488, 1243, 1200, 1172, 1106, 995, 872, 754, 679. ^{1}H NMR spectrum, δ, ppm: 2.32 t (2H, CH_2), 3.06–3.11 m (2H, CH_2), 3.98 br.s (2H, C_5H_4), 4.02 br.s (2H, C_5H_4), 4.06 s (5H, C_5H_5), 5.89 t (1H, NH), 7.04–7.06 m (4H, CH), 7.17–7.20 m (1H, CH), 7.40–7.43 m (2H, CH), 7.74 m (2H, CH), 9.72 s (1H, OH), 11.77 s (1H, OH). ^{13}C NMR spectrum, δ, ppm: 31.42, 44.02, 67.42, 68.13, 68.71, 85.85, 117.93, 119.60, 124.47, 126.83, 130.62, 131.85, 147.56, 150.91, 156.29, 157.67. Found, %: C 64.63; H 5.20; N 8.72. $C_{26}H_{25}N_3O_3Fe$. Calculated, %: C 64.60; H 5.21; N 8.69. MS: *m/z*: 482.724 $[M + H]^+$.

Synthesis of *vic*-dioxime complexes. A solution of one of the salts, $CdCl_2 \cdot 6H_2O$ (0.114 g, 0.5 mmol), $ZnCl_2$ (0.07 g 0.5 mmol), $NiCl_2 \cdot 6H_2O$ (0.059 g, 0.25 mmol), $CuCl_2 \cdot 2H_2O$ (0.043 g, 0.25 mmol), or $CoCl_2 \cdot 6H_2O$ (0.059 g, 0.25 mmol), in water (5 mL) was added to a solution of LH_2 (0.24 g, 0.5 mmol) in 5 mL of methanol at room temperature. A distinct change in color and a decrease in pH of the solution (2.5–3.0) were observed. While stirring at room temperature, NaOH (1%) was added to adjust pH to 7. The reaction mixture was stirred for 1 h at room temperature, then 2 mL of water were added to it. The resulting precipitate was filtered off, washed several times with water and dried in vacuum.

Cd(LH)(H_2O)(Cl). Yellow compound. Yield 30%, mp >250°C. FT-IR spectrum, ν, cm^{-1}: 3547, 3295, 3081, 3039, 2928, 1629, 1603, 1586, 1504, 1487, 1235, 1199, 1168, 1104, 999, 890, 869, 754, 691. ^{1}H NMR spectrum, δ, ppm: 2.31 t (2H, CH_2), 3.04–3.09 m (2H, CH_2), 3.97–3.99 m (2H, C_5H_4), 4.01–4.03 m (2H, C_5H_4), 4.06 br.s (5H, C_5H_5), 5.89 t (1H, NH), 7.03–7.07 m (4H, CH), 7.16–7.20 m (1H, CH), 7.40–7.44 m (2H, CH), 7.71–7.74 m (2H, CH), 11.77 s (1H, OH). ^{13}C NMR spectrum, δ, ppm: 31.41, 43.99, 67.40, 68.10, 68.70, 85.86, 117.95, 119.59, 124.46, 126.83, 130.62, 131.84, 147.56, 150.88, 156.29, 157.65. Found, %: C 48.24; H 4.01; N 6.43. $C_{26}H_{26}ClN_3O_4FeCd$. Calculated, %: C 48.18; H 4.04; N 6.48. MS: *m/z*: 648.098 $[M + H]^+$.

Zn(LH)(H_2O)(Cl). Yellow compound. Yield 35%, mp >250°C. FT-IR spectrum, ν, cm^{-1}: 3513, 3297, 3089, 3035, 2933, 1626, 1607, 1586, 1504, 1487, 1237, 1199, 1169, 1105, 1000, 891, 870, 756, 691. ^{1}H NMR spectrum, δ, ppm: 2.30 t (2H, CH_2), 3.04–3.10 m (2H, CH_2), 3.98–3.99 m (2H, C_5H_4), 4.02–4.03 m (2H, C_5H_4), 4.06 br.s (5H, C_5H_5), 5.89 t (1H, NH), 7.04–7.07 m (4H, CH), 7.16–7.20 m (1H, CH), 7.39–7.43 m (2H, CH), 7.71–7.73 m (2H, CH), 11.75 s (1H, OH). ^{13}C NMR spectrum, δ, ppm: 31.43, 43.91, 67.40, 68.11, 68.70, 85.87, 117.94, 119.59, 124.45, 124.75, 130.61, 131.83, 147.58, 152.26, 155.94, 157.65. Found, %: C 52.17; H 4.38; N 6.98. $C_{26}H_{26}ClN_3O_4FeZn$. Calculated, %: C 52.11; H 4.37; N 7.01. MS: *m/z*: 574.609 $[M + H - H_2O - OH]^+$.

Ni($LH)_2$. Dark reddish compound. Yield 71%, mp >250°C. FT-IR spectrum, ν, cm^{-1}: 3355, 3087, 3039, 2925, 1774, 1630, 1608, 1587, 1503, 1487, 1234, 1199, 1166, 1104, 1000, 902, 870, 742, 690. ^{1}H NMR spectrum, δ, ppm: 2.30 t (2H, CH_2), 3.05–3.08 m (2H, CH_2), 3.94–3.97 m (2H, C_5H_4), 3.98–4.01 m (2H, C_5H_4), 4.02 br.s (5H, C_5H_5), 5.85 t (1H, NH), 7.04–7.06 m (4H, CH), 7.18–7.20 m (1H, CH), 7.35–7.39 m (2H, CH), 7.40–7.45 m (2H, CH), 14.97 s (1H, OH). ^{13}C NMR spectrum, δ, ppm: 31.52, 45.14, 67.50, 68.21, 68.73, 85.12, 118.16, 119.85, 123.97, 124.67, 130.68, 131.75, 148.61, 151.13, 156.07, 158.02. Found, %: C 61.09; H 4.71; N 8.27. $C_{52}H_{48}N_6O_6Fe_2Ni$. Calculated, %: C 61.03; H 4.73; N 8.21. MS: *m/z*: 1023.807 $[M + H]^+$.

Scheme 1. Synthesis of LH_2 and the numbering of carbon atoms for 1D NMR (^1H and ^{13}C NMR) and 2D NMR (HSQC and HMBC) spectra.

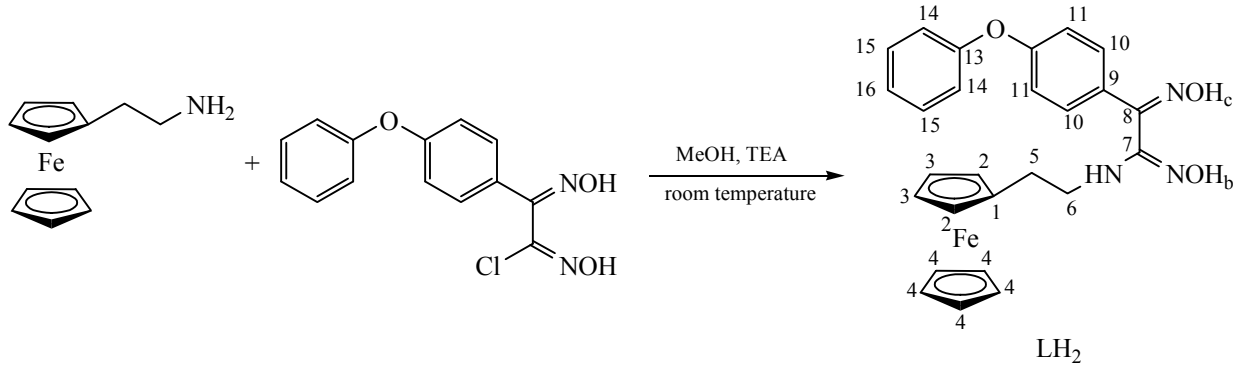

LH_2

$Cu(LH)_2$. Dark green compound. Yield 42%, mp 188°C. FT-IR spectrum, ν, cm^{-1}: 3380, 3080, 3035, 2962, 1773, 1637, 1603, 1586, 1503, 1487, 1235, 1196, 1167, 1104, 1000, 905, 869, 754, 691. Found, %: C 60.70; H 4.76; N 8.14. $C_{52}H_{48}N_6O_6Fe_2Cu$. Calculated, %: C 60.74; H 4.71; N 8.17. MS: *m/z*: 1028.192 $[M + H]^+$.

$Co(LH)_2(H_2O)_2$. Brown compound. Yield 40%, mp >250°C. FT-IR spectrum, ν, cm^{-1}: 3400, 3384, 3091, 3035, 2930, 1771, 1632, 1607, 1586, 1504, 1487, 1233, 1198, 1167, 1104, 1000, 905, 870, 745, 691. Found, %: C 58.61 H 4.85; N 7.87. $C_{52}H_{52}N_6O_8Fe_2Co$. Calculated, %: C 58.69; H 4.93; N 7.92. MS: *m/z*: 1027.557 $[M - 2H_2O]^+$.

Theoretical calculations. Initially the molecular geometries of LH_2 ligand and its Cd(II), Zn(II), and Ni(II) complexes were optimized. This was followed by calculations of electric dipole moments, static dipole polarizabilities and first hyperpolarizabilities. Dispersion-free α and β were calculated using the FF scheme [28]. The cep-4*g* basis set [29, 30] has been found adequate for obtaining reliable hyperpolarizability values. All geometry optimizations, μ, static α and β calculations were performed by GAUSSIAN 03W [31] program at the HF level with cep-4*g* basis set. The averaged (isotropic) dipole polarizability ⟨α⟩ and the magnitude of β_{tot} (total first static hyperpolarizability) were calculated using the following expressions, respectively [32, 33]:

$$\langle\alpha\rangle = (\alpha_{xx} + \alpha_{yy} + \alpha_{zz})/3, \quad (1)$$

$$\beta_{tot} = [(\beta_{xxx} + \beta_{xyy} + \beta_{xzz})^2 + (\beta_{yyy} + \beta_{yzz} + \beta_{yxx})^2 + (\beta_{zzz} + \beta_{zxx} + \beta_{zyy})^2]^{1/2}, \quad (2)$$

where the components of first hyperpolarizability tensor β_i ($i = x, y, z$) are given by:

$$\beta_i = \beta_{iii} + 1/3\sum_{i\neq j}(\beta_{ijj} + \beta_{jij} + \beta_{jji}). \quad (3)$$

To understand the relationship of NLO properties with the molecular structure, HOMOs, LUMOs and HOMO-LUMO gaps of LH_2 ligand and its Cd(II), Zn(II), Ni(II) complexes have been generated by GAUSSIAN03W [31] program utilizing the HF method with cep-4*g* basis set.

RESULTS AND DISCUSSION

Characterization of *vic*-dioxime ligand and its complexes. The synthesized ligand (LH_2) [32] (Scheme 1) and its metal complexes (Scheme 2) structures were characterized by FT-IR, UV-Vis, 1D NMR (^1H, ^{13}C), 2D NMR (HMBC), and ESI mass spectrometry. Elemental analyses and ESI mass spectrometry of the complexes indicated that the metal–ligand ratios were 1 : 2 or 1 : 1, and their formulas were determined to be as follows: $[M(LH)_2]$ [M=Ni(II) or Cu(II)], $[M(LH)_2(H_2O)_2]$ [M=Co(II)], and [M(LH)(H_2O)CI] [M = Zn(II) or Cd(II)] (Scheme 2).

In the ^1H NMR spectrum of LH_2, the amino group signal of β-ferrocenylethylamine was not recorded, instead the new signal at 5.89 ppm attributed to NH indicated that β-ferrocenylethylamine condensed with 4-(phenoxy)chlorophenylglyoxime. The chemical shifts of C=N–OH protons (9.72 and 11.77 ppm) of the ligand disappeared upon addition of D_2O, confirming the (*E,E*)-form of the *vic*-dioxime [34]. The ^1H NMR spectrum of $Ni(LH)_2$ supported formation of an intramolecular H-bridge, the new signal of which was measured at 14.97 ppm. In ^1H NMR spectra of Cd and Zn complexes, the signals of N–OH were measured at 11.74 and 11.75 ppm, respectively. The other chemical shifts arising from the aromatic, aliphatic and ferrocenyl protons were similar to those of the free ligand. Paramagnetic nuclei of Cu^{+2} and Co^{+2}

Scheme 2. The general formulae of the complexes.

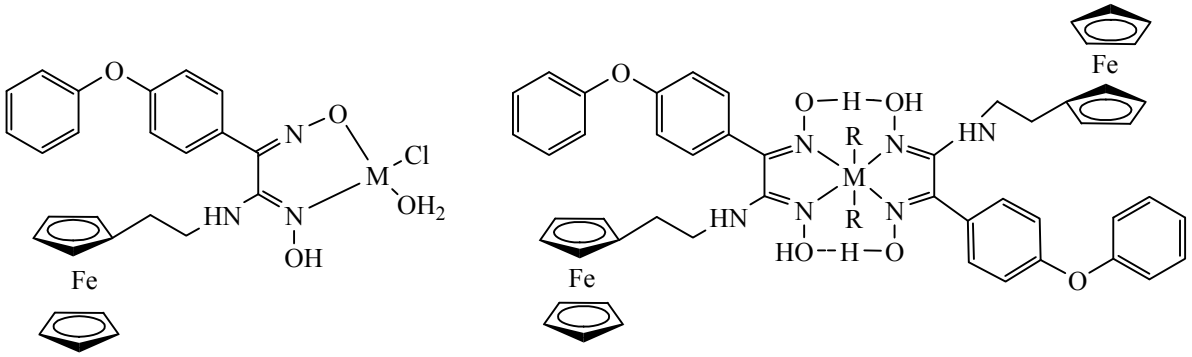

M = Cd, Cd(LH)(H_2O)(Cl)
M = Zn, Zn(LH)(H_2O)(Cl)

M = Ni, $Ni(LH)_2$
M = Cu, $Cu(LH)_2$
M = Co, R = H_2O, $Co(LH)_2(H_2O)_2$

broadened the ^{1}H NMR signals of the ligand making it difficult to identify and attribute those. Upon complexation with Ni(II), Cd(II), and Zn(II) cations, the ligand resonances shifted slightly as expected. Structure of the ligand was supported also by the 2D HSQC and HMBC spectrum (Table 1). IR spectra of the products were in good agreement with the above data. UV–Vis spectra of the ligand and its complexes in DMSO indicated two or three absorption bands between 260 and 550 nm. Spectra of compounds (Fig. 1) demonstrated the intense absorption at 275 and 320 nm, that could be attributed to $\pi\rightarrow\pi^*$ transitions of the aromatic ring and $n\rightarrow\pi^*$ transitions, respectively [35]. The spectrum of $Ni(LH)_2$ exhibited less intense absorption bands in the range of 460–510 nm that could be attributed to *d–d* transitions of the square

Table 1. ^{13}C NMR, ^{1}H–^{13}C HSQC and ^{1}H–^{13}C HMBC data for LH_2

Carbon atoms number	δ_C, ppm	^{1}H–^{13}C HSQC (^1J)	^{1}H–^{13}C HMBC ^2J–^4J
1	85.85	–	4.02 (H_2), 3.98 (H_3), 2.32 (H_5)
2	67.42	4.02 (H_2)	3.98 (H_3), 2.32 (H_5)
3	68.13	3.98 (H_3)	4.02 (H_2),2.32 (H_5)
4	68.71	4.06 (H_4)	–
5	31.42	2.32 (H_5)	–
6	44.02	3.06–3.11 (H_6)	2.32 (H_5)
7	147.56	–	5.89 (H_a), 11.77 (H_c)
8	150.91	–	9.72 (H_b)
9	126.83	–	7.74 (H_{10}), 7.04–7.06 (H_{11})
10	131.85	7.74 (H_{10})	7.04–7.06 (H_{11})
11	117.93	7.04–7.06 (H_{11})	7.74 (H_{10}), 7.04–7.06 (H_{14})
12	157.67	–	7.74 (H_{10}), 7.04–7.06 (H_{11})
13	156.29	–	7.04–7.06 (H_{14}), 7.40–7.43 (H_{15})
14	119.60	7.04–7.06 (H_{14})	7.40–7.43 (H_{15}), 7.17–7.20 (H_{16})
15	130.62	7.40–7.43 (H_{15})	7.17–7.20 (H_{16}), 7.04–7.06(H_{14})
16	124.47	7.17–7.20 (H_{16})	7.04–7.06 (H_{14}), 7.40–7.43 (H_{15})

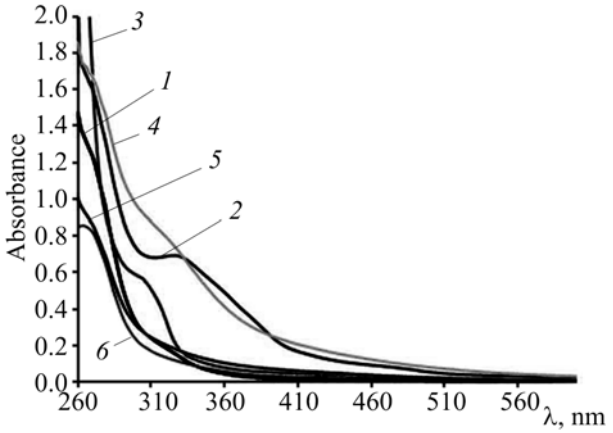

Fig. 1. UV-Vis spectra of the (*1*) LH_2 and its metal complexes [(*2*) $Ni(LH)_2$, (*3*) $Cu(LH)_2$, (*4*) $Co(LH)_2(H_2O)_2$, (*5*) $Cd(LH)(H_2O)(Cl)$, (*6*) $Zn(LH)(H_2O)(Cl)$] in DMSO solution (1×10^{-4} M).

planar structure [36]. The weak *d–d* transition of copper and cobalt complexes were not recorded [37].

Electrochemical studies. The redox properties of LH_2 and its metal complexes were studied using CV. LH_2 and its metal complexes 10^{-3} M solutions in anhydrous DMSO (0.1 M TBATFB) were prepared. The voltammograms were recorded at 100 mV/s from 1.0 to –2.5 V, and demonstrated a well-defined pair of symmetric peaks, an anodic peak, and the corresponding cathodic peak located at ca +0.50 V, that stemed from the redox active ferrocenyl substituents (Table 2). The peak potentials and peak currents were not significantly influenced by the structural changes in the *vic*-dioxime derivatives, which meant that the ferrocene redox centers were well isolated from the *vic*-dioxime moieties. The cyclic voltammogram of LH_2 demonstrated the ferrocene couple at 0.51 V along with an irreversible peak at –1.85 V that could be ascribed to oxime-centered reduction [38]. For the Ni(II) complex apart from the ferrocene couple at about 0.53 V, the voltammogram displayed reduction at –1.23 V, which was characteristic to Ni(II)/Ni(I) reduction [39]. Reduction of oxime moieties was achieved at E_{pc}: –1.95 and –1.85 V for the Co(II) and Cd(II) complexes, respectively. Absence of a reduction peak of the oxime group for $Ni(LH)_2$, $Cu(LH)_2$ and $Zn(LH)(H_2O)(Cl)$ indicated that reduction potentials of the dianionic ligands shifted beyond the lower limit of the potential interval considered in the experimental measurements because of the lack of transferable hydroxylic protons [40]. The reversible Fc···Fc redox process of Cu(II) complexes ($E_{1/2}$ = 0.55) shifted, compared with the ligand ($E_{1/2}$ = 0.51). Probably Cu(II) ion electron accepting ability could lead to the decrease of electron density of the ferrocenyl moiety and increased electron delocalization in the whole molecule. So, the metal complexes were less prone to oxidation than the ligand [41].

Second-order NLO properties of the *vic*-dioxime ligand and its Cd(II), Zn(II), and Ni(II) complexes.

Table 2. Voltammetric data for the compounds in DMSO (TBATFB)

Compound	Redox couple	E_{pa},[a] V	E_{pc},[b] V	ΔE_p, V	$E_{1/2}$[c,d] or E_p,[e] V
LH_2	Fc/Fc^+ Ox/Ox^-	0.54	0.47	0.07	0.51 –1.85
$Ni(LH)_2$	Fc/Fc^+ Ox/Ox^-	0.59	0.47	0.12	0.53
$Cu(LH)_2$	Fc/Fc^+ Ox/Ox^-	0.62	0.49	0.13	0.55
$Co(LH)_2(H_2O)_2$	Fc/Fc^+ Ox/Ox^-	0.58	0.47	0.11	0.53 –1.95
$Cd(LH)(H_2O)(Cl)$	Fc/Fc^+ Ox/Ox^-	0.54	0.47	0.07	0.51 –1.89
$Zn(LH)(H_2O)(Cl)$	Fc/Fc^+ Ox/Ox^-	0.55	0.47	0.08	0.52

[a] (E_{pa}) anodic peak potential. [b] (E_{pc}) cathodic peak potential. [c] Half-wave ($E_{1/2}$) or peak (E_p) potentials in DMSO/TBATFB versus Fc/Fc^+couple correspond approximately to the above data – 0.50 V. Data were acquired by cyclic voltammetry. [d] $E_{1/2}$= (E_{pa}+E_{pc})/2 for reversible or quasi-reversible processes. [e] (E_p) indicates the cathodic peak potential for irreversible reduction processes and the anodic peak potential for irreversible oxidation processes.

The high dipole moment values are associated, in general, with larger projection of β_{tot} quantities. Connection of the electric dipole moment of a molecule with first hyperpolarizability is widely recognized [42, 43]. Researchers tried to identify the molecules with potentially optimal nonlinearities by means of the Two-Level model. For example, Gorman et al. [44] used a four-site Hückel Model to examine how each of the Two-Level parameters varied with the electron-donating and electron-accepting abilities of appended substituents. One of their conclusions was that non-zero μ value might permit to find non-zero β value. In this study, the static dipole polarizabilities and first hyperpolarizabilities, respectively, were computed by the numerical first and second derivatives of the electric dipole moments according to the applied field strength in FF approach. The electric dipole moments, selected values of the static dipole polarizabilities and first hyperpolarizabilities computed for LH_2 ligand and its Cd(II), Zn(II), Ni(II) complexes are listed in Tables 3–5. There is a strong relationship among the calculated μ, ⟨α⟩ and β_{tot} values. Therefore, rather high μ values (Table 3) may be responsible for enhancing ⟨α⟩ and β_{tot} values (Tables 4, 5). Com-plexes of Cd(II), Zn(II) and Ni(II) with LH_2 ligand had similar structures except transition metal centres, but large differences between the corresponding static dipole polarizabilities and first hyperpolarizabilities existed. Among Cd(II), Zn(II) and Ni(II) complexes, the latter one exhibited the highest ⟨α⟩ and β_{tot} (Tables 2, 3).

We have also examined the HOMO and LUMO energies of LH_2 ligand and its Cd(II), Zn(II) and Ni(II) complexes. The HOMO and LUMO energies and HOMO–LUMO energy gaps determined by the HF method are listed in Table 6. The selective frontier and second frontier molecular orbitals for the compounds are presented in Figs. 2, 3. According to these, HOMO-1 refered to the second highest occupied molecular orbital. The second and third-order NLO responses could be dictated by charge-transfer excitations involving the HOMO and LUMO orbitals in such a way that the larger values of first and second hyperpolarizabilities should correspond to lower HOMO–LUMO gaps. The hyperpolarizabilities were, therefore, directly related to the HOMO–LUMO energy gap. It was evident that there should have been an inverse relationship between the HOMO–LUMO gap and hyperpolarizability values [45]. The best values of hyperpolarizabilities could be achieved with lower HOMO–LUMO gaps. So, it could be expected

Table 3. The ab initio calculated electric dipole moments μ and dipole moment components for LH_2 ligand and its $Ni(LH)_2$, $Cd(LH)(H_2O)(Cl)$, and $Zn(LH)(H_2O)(Cl)$ complexes

Compound	μ_x, D	μ_y, D	μ_z, D	μ, D
LH_2	0.069	2.305	–0.238	2.318
$Ni(LH)_2$	–0.089	1.745	2.016	2.668
$Cd(LH)(H_2O)(Cl)$	6.429	–4.072	0.701	7.642
$Zn(LH)(H_2O)(Cl)$	5.961	–5.130	0.134	7.866

Table 4. Some selected components of the static α(0; 0) and ⟨α⟩(0; 0) ($\times 10^{-24}$ esu) values for LH_2 ligand and its $Ni(LH)_2$, $Cd(LH)(H_2O)(Cl)$, $Zn(LH)(H_2O)(Cl)$ complexes

Compound	α_{xx}	α_{yy}	α_{zz}	⟨α⟩
LH_2	47.780	29.979	29.146	35.635
$Ni(LH)_2$	101.797	67.637	56.507	75.314
$Cd(LH)(H_2O)(Cl)$	53.019	35.161	30.474	39.551
$Zn(LH)(H_2O)(Cl)$	50.746	34.475	30.952	38.724

Table 5. Some selected components of the static β(0;0,0) and $\beta_{tot}(0;0,0)$($\times 10^{-30}$ esu) values for LH_2 ligand and its $Ni(LH)_2$, $Cd(LH)(H_2O)(Cl)$ and $Zn(LH)(H_2O)(Cl)$ complexes

Compound	β_x	β_y	β_z	β_{tot}
LH_2	–1.635	1.703	–0.753	2.479
$Ni(LH)_2$	0.904	1.449	1.929	2.577
$Cd(LH)(H_2O)(Cl)$	0.225	0.897	–1.942	2.152
$Zn(LH)(H_2O)(Cl)$	0.740	0.703	–1.706	1.988

that the Ni(II) complex with the lowest HOMO–LUMO gaps (0.343 and 0.371 a.u. for first and second frontier molecular orbitals, respectively) could give the highest value for β_{tot} for LH_2 ligand (Tables 5, 6). The HOMO and HOMO-1 of LH_2 were localized on the six-membered rings, single and double bonds attached to the aromatic and ferrocene units, while the LUMO and LUMO+1 were mainly located on the aromatic benzene rings (Fig. 2). The electron distributions of frontier and second frontier molecular orbitals for Cd(II) and Zn(II) complexes were almost similar and placed on the metal cores, six-membered rings, single and double bonds attached to the aromatic and ferrocene units, whereas the electron densities on the Ni(II) complex were located predominantely on the metal core (Fig. 3).

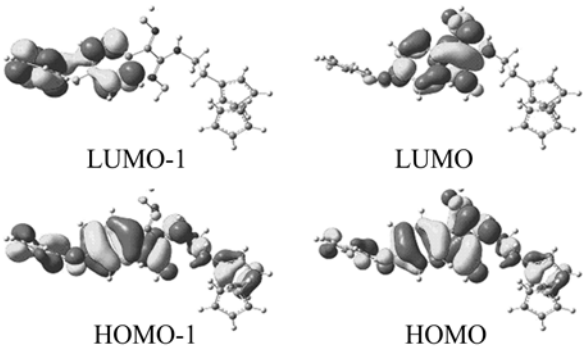

Fig. 2. Frontier and second frontier molecular orbitals of LH_2 ligand.

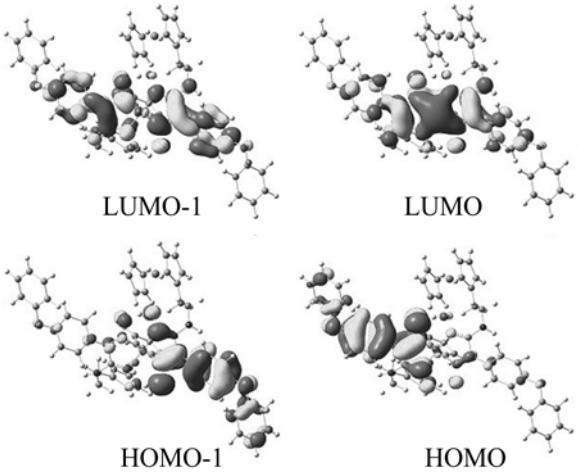

Fig. 3. Frontier and second frontier molecular orbitals of $Ni(LH)_2$ complex.

Table 6. Calculated HOMO-LUMO energy (a.u.) and HOMO-LUMO band gap (E_g) values for LH_2 ligand and its $Ni(LH)_2$, $Cd(LH)(H_2O)(Cl)$ and $Zn(LH)(H_2O)(Cl)$ complexes

Parameter	LH_2	$Ni(LH)_2$	$Cd(LH)(H_2O)(Cl)$	$Zn(LH)(H_2O)(Cl)$
HOMO	–0.345	–0.337	–0.330	–0.336
LUMO	0.043	0.006	0.047	0.040
E_g(LUMO – HOMO)	0.388	0.343	0.377	0.376
HOMO-1	–0.349	–0.339	–0.359	–0.362
LUMO+1	0.081	0.031	0.069	0.067
E_g[(LUMO+1) – (HOMO-1)]	0.430	0.370	0.428	0.429

CONCLUSIONS

The new ferrocene-substituted *vic*-dioxime ligand and its Ni(II), Cu(II), Co(II), Cd(II), and Zn(II) complexes are synthesized and their structures are evaluated. According to the spectroscopic data, the tetrahedral geometry of the Cd(II) and Zn(II) complexes, an octahedral geometry of the Co(II) complex, and a square-planar geometry of Ni(II) and Cu(II) complexes are proposed. Redox behavior of the complexes is explored with CV based on the metal-centered reduction processes. The *ab initio* calculated non-zero μ and β_{tot} values imply that LH_2 ligand and its Cd(II), Zn(II), Ni(II) complexes may have microscopic second-order NLO phenomena. The highest values for $\langle\alpha\rangle$ and β_{tot} are obtained for Ni(II) complex, indicating its suitability as potential material for second-order NLO applications. The Ni(II) complex displays the lowest HOMO-LUMO gaps, confirming an inverse correlation with its $\langle\alpha\rangle$ and β_{tot} values.

FUNDING

This work was supported by TUBITAK (Scientific and Technological Research Council of Turkey) with project numbers of 111T970 and SÜ BAP with projects numbers of 13401023 and 18701120.

CONFLICT OF INTEREST

No conflict of interest was declared by the authors.

REFERENCES

1. Silva, P.A., Maria, T.M.R., Nunes, C.M., Eusébio, M.E.S., and Fausto, R., *J. Mol. Struct.*, 2014, vol. 1078, p. 90. doi 10.1016/j.molstruc.2013.12.031

2. Gupta, S.R., Mourya, P., Singh, M.M., and Singh, V.P., *J. Organomet. Chem,*. 2014, vol. 767, p. 136. doi 10.1016/j.jorganchem.2014.05.038
3. Paitandi, R.P., Gupta, R.K., Singh, R.S., Sharma, G., Koch, B., and Pandey, D.S., *Eur. J. Med. Chem*., 2014, vol. 84, p. 17. doi 10.1016/j.ejmech.2014.06.052
4. Chinnadayyala, S.R., Kakoti, A., Santhosh, M., and Goswami, P., *Biosen. Bioelectron*., 2014, vol. 55, p. 120. doi 10.1016/j.bios.2013.12.005
5. Dervisevic, M., Dervisevic, E., Senel, M., Cevik, E., Yildiz, H.B., and Camurlu, P., *Enzyme Microb. Tech*., 2017, vol. 102, p. 53. doi 10.1016/j.enzmictec.2017.04.002
6. Rabti, A., Mayorga-Martinez, C.C., Baptista-Pires, L., Raouafi, N., and Merkoçi, A., *Anal. Chim. Acta*, 2016, vol. 926, p. 28, 10.1016/j.aca.2016.04.010
7. Zhu, P., Kan, L., Han, X., Feng, J., Jia, J., and Zhang, X., *Dyes Pigments*, 2015, vol. 113, p. 55. doi 10.1016/j.dyepig.2014.07.009
8. Congiu, M., Nunes-Neto, O., De Marco, M.L., Dini, D., and Graeff, C.F.O, *Thin Solid Films*, 2016, vol. 612, p. 2. doi 10.1016/j.tsf.2016.05.033
9. Wua, Y., Kashia, M.B., Yanga, Y., Gonçalesa, V.R., Ciampid, S., Tilleya, R.D., and Gooding, J., *Electrochim. Acta*, 2016, vol. 213, p. 540. doi 10.1016/j.electacta.2016.07.120
10. Zhang ,L., Chen, H., Zhao, X., Zhai, Q., Yina, D., Sunb, Y., and Li, J., *Appl. Catal. B: Environ*., 2016, vol. 193, p. 47. doi 10.1016/j.apcatb.2016.04.019
11. Dixit, S., Siddiqui, Q.T., Muneer, M., and Agarwal, N., *Tetrahedron Lett*., 2016, vol. 57, p. 4228. doi 10.1016/j.tetlet.2016.08.020
12. Mbaba, M., Mabhula, A.N., Boel, N., Edkins, A.L., Isaacs, M., Hoppeb, H.C., and Khanye, S.D., *J. Inorg. Biochem*., 2017, vol. 172, p. 88. doi 10.1016/j.jinorgbio.2017.04.014
13. Moriuchi, T., Nishiyama, T., Tayano, Y., Tohnai, N., and Hirao, T., *J. Organometal. Chem*., 2017, vol. 839, p. 78. doi 10.1016/j.jorganchem.2017.01.005
14. Matei, A., Constantinescu, C., Ion, V., Mitu, B., Ionita, I., Dinescu, M., Vasiliu, C., and Emandi, A., *J. Organomet. Chem*., 2014, vol. 751, p. 638. doi 10.1016/j.jorganchem.2013.10.056
15. Kaur, S., Kaur, M., Kaur, P., Clays, K., and Singh, K., *Coord. Chem. Rev*., 2017, vol. 343, p. 185. doi 10.1016/j.ccr.2017.05.008
16. Deveci, P. and Taner, B., *Inorg. Chim. Acta*, 2013, vol. 405, p. 326. doi 10.1016/j.ica.2013.06.012
17. Harbeck, M., Şen, Z., Gümüş, G., Gürol, I., Musluoğlu, E., Öztürk, Z.Z., and Ahsen, V., *Sens. Actuators B*, 2013, vol. 188, p. 1004. doi 10.1016/j.snb.2013.08.014
18. Musılova, L., Kuca, K., Jung, Y.S., and Jun, D., *Clin. Toxicol*, 2009, vol. 47, p. 545. doi 10.1080/15563650903058914
19. Mokhir, A., Kraamer, R., Voloshin, Y.Z., and Varzatskii, O.A., *Bioorg. Med. Chem. Lett*., 2004, vol. 14, p. 2927. doi 10.1016/j.bmcl.2004.03.028
20. Mandal, D. and Gupta, B.D., *Organometal*., 2006, vol. 25, p. 3305. doi 10.1021/om060357x
21. Pantani, O., Anxolabehere-Mallart, E., Aukauloo, A., and Millet, P., *Electrochem. Commun*., 2007, vol. 9, p. 54. doi 10.1016/j.elecom.2006.08.036
22. Moloney, J.V., *Nonlinear Optical Materials*, New York: Springer, 1998.
23. Lednicer, D. and Hauser, C.R., *Org. Synth*., 1973, vol. 5, p. 434. doi 10.15227/orgsyn.040.0031
24. Lednicer, D. and Hauser, C.R., *Org. Synth*., 1973, vol. 5, p. 578.
25. Lednicer, D., Lindsay, J.K., and Hauser, C.R., *J. Org. Chem.*, 1958, vol. 23, p. 653. doi 10.1021/jo01099a700
26. Cavallini, G., Massarani, E., Nardi, D., Mauri, L., Tenconi, F., Pacchiano, P., and Mantegazza, P., *J. Med. Chem*., 1963, vol. 6, p. 573
27. Coşkun, A., Yılmaz, F., and Akgemci, E.G., *J. Incl. Phenom. Macrocycl. Chem*., 2008, vol. 60, p. 393. doi 10.1007/s10847-007-9389-x
28. Kurtz, H.A., Stewart, J.P.P., and Dieter, K.M., *J. Comput. Chem*., 1990, vol. 11, p. 82. doi 10.1002/jcc.540110110
29. Stevens, W., Basc, H., and Krauss, J., *J. Chem. Phys*., 1984, vol. 81, p. 6026. doi 10.1063/1.447604
30. Cundari, T.R. and Stevens, W.J., *J. Chem. Phys.*, 1993, vol. 98, p. 5555. doi 10.1063/1.464902
31. Frisch, M.J., *Gaussian 03*, Revision E.01, Gaussian, Inc., Wallingford CT, 2004.
32. Bogaard, M.P. and Orr, B.J., *MTP International Review of Science*, Buckingham, A.D., Ed., London: Butterworths, 1975, vol. 2, p. 149.
33. Thanthiriwatte, K.S. and de Nalin, K.M., *J. Mol. Struct*., 2002, vol. 617, p. 169. doi 10.1016/S0166-1280(02)00419-0
34. Yuksel, F., Gurek, A.G., Durmuş, M., Gurol, İ, Ahsen, V., Jeanneau, E., and Luneau, D., *Inorg. Chim. Acta*, 2008, vol. 361, p. 2225. doi 10.1016/j.ica.2007.11.019
35. Kandaz, M. and Katmer, O., *Trans. Met. Chem*., 2006, vol. 31, p. 889.
36. Shaabani, B. and Shaghaghi, Z., *Appl. Organomet. Chem*., 2011, vol. 25, p. 317. doi 10.1002/aoc.1761
37. Karipçin, F., Dede, B., Percin Özkorucuklu, S., and Kabalcilar, E., *Dyes Pigments,* 2010, vol. 84, p. 14. doi 10.1016/j.dyepig.2009.06.010
38. Uçar, A., Deveci, P., Taner, B., Fındık, M., Bereket, S., Özcan, E., and Solak, A.O., *J. Coord. Chem*., 2010, vol. 63, p. 3083. doi 10.1080/00958972.2010.504259

39. Çamur, M., Bulut, M., Ozkaya, A.R., Kandaz, M., and Yaylı, N., *Trans. Met. Chem*., 2007, vol. 32, p. 642.
40. Isse, A.A., Gennaro, A, and Vianello, E., *Electrochim. Acta*, 1997, vol. 42, p. 2065. doi 10.1016/S0013-4686 (97)85482-5
41. Wu, D., Xiao, L., Shi, Y., Zhang, Q, Du, W., Zhang, J., Li, S., Zhou, H., Wu, J., and Tian, Y., *J. Organomet. Chem*., 2017, vol. 830, p. 67. doi 10.1016/ j.jorganchem.2016.12.012
42. Prasad, P.N. and Williams, D.J., *Introduction to Nonlinear Optical Effects in Organic Molecules and Polymers*, New York: Wiley, 1991.
43. *Nonlinear Optical Properties of Organic Molecules and Crystals*, Chemla, D.S. and Zyss, J., Eds., New York: Academic Press, 1987.
44. Gorman, C.B. and Marder, S.R., *Proceeding of the National Academy of Sciences of the United States of America*, 1993, vol. 90, p. 11297.
45. Liyanage, P.S., de Silva, R.M., and Nalin de Silva, K.M., *J. Mol. Struct. (Theochem.)*, 2003, vol. 639, p. 195.